J Sol-Gel Sci Technol (2009) 52:31–40
DOI 10.1007/s10971-009-2010-6

ORIGINAL PAPER

Corrosion protection of aluminium alloy AA2024 with cerium doped methacrylate-silica coatings

N. C. Rosero-Navarro · S. A. Pellice · A. Durán · S. Ceré · M. Aparicio

Received: 19 December 2008 / Accepted: 28 May 2009 / Published online: 17 June 2009

Abstract The aim of this work is the synthesis and characterization of hybrid coatings doped with cerium salts for corrosion protection of AA2024. The control of the inorganic and organic polymerization process allows the preparation of coatings with an open structure and a hydrophilic character. These facts facilitate the incorporation and mobility of cerium ions through the structure, enhancing its ability to promote a self-healing mechanism. The thermal treatment of the coatings has been limited to 120 °C to preserve the mechanical properties of the alloy. The electrochemical behaviour of the coatings has been evaluated in 0.3 wt% NaCl solution by means of EIS technique. Electrochemical measurements evidence good barrier properties at initial immersion time, and signals of corrosion inhibition from cerium ions at long immersion times could be assigned to the increasing of the impedance modulus at low frequencies and the presence of cerium oxide/hydroxide precipitates.

Keywords Sol–gel · Hybrid coatings · Cerium · Inhibitors · AA2024 · EIS

N. C. Rosero-Navarro · S. A. Pellice · A. Durán · M. Aparicio (✉)
Instituto de Cerámica y Vidrio (CSIC), Campus de Cantoblanco, 28049 Madrid, Spain
e-mail: maparicio@icv.csic.es

S. A. Pellice · S. Ceré
INTEMA, Universidad Nacional del Mar del Plata-CONICET, Juan B. Justo 4302, B7608FDQ Mar del Plata, Argentina

1 Introduction

The protection of aluminium alloys from corrosion in chemically aggressive environments is a difficult issue that limits the applications of these alloys in different fields. Aluminium alloy AA2024 has very interesting mechanical properties and is usually applied in aircraft design. The environments and conditions this alloy is subject to results in a challenging problem of corrosion protection, especially from pitting corrosion. One of the best strategies to improve the corrosion resistance is the use of coatings with the incorporation of corrosion inhibitors. Cr(VI) compounds, mainly chromates, are among the most common substances used, and their high efficiency/cost ratio has made them standard corrosion inhibitors [1]. The generally accepted model for precipitation of chromate conversion coatings is via a redox reaction between chromate ions in solution and aluminium, resulting in the formation of a hydrated chromium oxide gel on the surface of the alloy [2]. However, chromates are considered as potential lung carcinogen responsible for DNA damage and make them environmentally hostile. So, an intense effort is being undertaken to replace them [3]. Cerium compounds seem to fulfil the basic requirements for consideration as alternative corrosion inhibitors: the ions form insoluble hydroxides which enable them to be used as cathodic inhibitors; they have a low toxicity, and are relatively abundant in nature [4–6]. Some papers [7–9] propose that when the oxygen reduction reaction occurs at activated cathodic site producing OH^- groups, the pH increases in the vicinity of the sites giving rise to the precipitation of $Ce(OH)_3$.

An alternative to chromate conversion coatings (CCC) can be the synthesis of sol–gel coatings sintered at temperatures lower than 500 °C. Different sol–gel coatings have been developed to increase the corrosion resistance of

metals, although the pure inorganic films have limitations such as micro cracks, residual porosity and thickness limitations. The incorporation of non-hydrolysable groups, as for example methyl groups through methyltriethoxysilane (MTES), has reduced some of these limitations [10]. An important parameter to be considered is the thermal treatment required for the film consolidation. For glass-like coatings, temperature has to be high enough to ensure the ceramic bonding between film and substrate as well as the densification of the film through the network consolidation and pore elimination. Indeed, the sintering schedule must take into account the properties of the substrate; therefore, some limits must be respected in order to keep the desirable character of the film and the integrity of the metal base.

Some metals and alloys present structural changes with temperature, with formation of precipitates, structural evolution, etc. that degrade the mechanical properties and corrosion resistance. In these cases, systems with sintering temperatures preserving the integrity of the substrate must be used taking care that coating treatment induces no degradation of the substrate. For example, the temperature of thermal treatment for coatings on aluminium alloy AA2024 can not be higher than 120 °C. This circumstance limits the application of inorganic sol–gel coatings suitable to increase the corrosion protection of these alloys [10].

The development of hybrid organic-inorganic sol–gel coatings where an organic network is promoted together with an inorganic one can lead to consolidated structures at significantly lower temperatures compared with traditional inorganic sol–gel coatings. The preparation of this hybrid structure needs a severe synthesis control of all parameters involved in the process to obtain a homogeneous interpenetration of both networks with no phase separation. Organically modified silicon alkoxides with organic polymerisable groups attached to the silicon atom are now available. Most of papers published [10] exploit a strategy based on epoxy groups attached to silicon to promote the synthesis of the organic network. Different aluminium alloys have been coated with epoxy based sol–gel coatings [10–16] treated with sintering temperatures below 200 °C. The coatings protect these alloys against aggressive electrolytes although degradation was observed at long immersion times as a consequence of the water intake experienced.

Recently, a new research trend in sol–gel process is oriented to the development of sol–gel coatings doped with environmentally friendly inhibitors as cerium compounds [17–29]. These systems try to combine the "barrier protection" effect of sol–gel coatings with the "corrosion inhibitor" effect of the cerium ions inside the coatings. Sol–gel coatings used as barriers prevent contact between the metal surface and corrosive species. Active protection with cerium would imply that corrosion is inhibited by cerium ions that migrate through the coating to the site of the attack (a defect in the coatings) and then react to passivate the site. Hybrid silica coatings prepared with TEOS and MTES doped with cerium salts, $Ce(NO_3)_3$ and $(NH_4)_2Ce(NO_3)_6$, on stainless steel and aluminium substrates present an improvement in corrosion protection with increased immersion time in NaCl solutions. The explanation of this behaviour is the precipitation of a mixed cerium (III and IV) and chromium (in the case of stainless steel) hydroxides-oxides on cathodic areas by reaction with hydroxyl groups triggered by an increase of pH [17, 18]. Silica based sol–gel coatings doped with $Ce(NO_3)_3$ on galvanized steel substrates have also showed the protective behaviour of these coatings. EIS and scanning vibrating electrode technique (SVET) studies of this system with an artificial defect created on its surface have demonstrated signals of self-healing effect [19, 20].

In the case of corrosion protection of aluminium alloys with sintering processes limited at temperatures as low as 120 °C, as AA2024 alloy, sol–gel coatings based on epoxy functional groups and doped with cerium have been developed. This composition guarantees a good compatibility and bonding with the epoxy based primer or topcoat typically used with aluminium substrates. Moreover, the availability of silica sol–gel precursors with an epoxy functional group makes easy the chemical bonding between the sol–gel coating and the substrate. Some works [21–25] have utilized cerium nitrate into the epoxy based sol–gel coatings. Results have showed an improvement of corrosion resistance in NaCl solutions at low immersion times. Initial analysis indicates the increase of impedance at low frequencies as a signal of self-healing effect. However, the combination of both kinds of properties (barrier and inhibition) in the same coating is a very difficult issue. The barrier functionality is based on a highly cross-linked structure that would be inefficient for a fast diffusion of cerium ions through it.

An almost unexplored way of preparation of hybrid sol–gel coatings with two (organic and inorganic) interpenetrating networks can be sustained by the presence of vinyl groups attached to silicon atoms. These kinds of coatings would be thermally treated at low temperatures, as the epoxy based sol–gel coatings, and readily applied on aluminium substrates. Hybrid sol–gel coatings on aluminium substrates have been synthesized with vinyltrimethoxysilane (VMS) and 3-methacryloxypropyl trimethoxysilane (MPS) [26]. Polarization curves indicate a reduction of corrosion current of coated samples. However, the absence of an active corrosion inhibition limits the protection properties of these coatings with the immersion time.

The aim of this work was to study the synthesis and characterization of cerium doped hybrid organic-inorganic sol–gel coatings on aluminium alloy AA2024 using as precursors TEOS, MPS and 2-hydroxyethyl methacrylate

(HEMA). The incorporation of the monomer HEMA, with a hydroxyl group and a double bond susceptible to organic polymerisation compatible with the methacrylate group from MPS, open up the possibilities of synthesis of these coatings with a higher organic/inorganic ratio. The idea is the synthesis of an open structure to allow the fast diffusion of cerium ions. An important issue in this work is the study of the inhibition corrosion properties as a pre-treatment instead of CCC coatings. An overcoat painting on these coatings would provide the barrier functionality.

2 Experimental

The precursor sols were synthesized using 2-hydroxyethyl methacrylate (HEMA, Aldrich, 97%), 3-methacryloxypropyl trimethoxysilane (MPS, ABCR, 98%), and tetraethoxysilane (TEOS, ABCR, 98%). A 0.1N HNO_3 solution was used as catalyst. The initiator of the organic polymerization was 2,2′-azobis (isobutyronitrile) (AIBN, Aldrich, 98%). Cerium chloride ($CeCl_3 \cdot 7H_2O$, Aldrich, 99.9%) and cerium nitrate ($Ce(NO_3)_3 \cdot 6H_2O$, Aldrich, 99%) were used as sources of Ce(III). Ethanol (Panreac, analytical grade) was employed as solvent. Glass slides (2×7 cm^2) and AA2024 aluminium alloy (5×7 cm^2) were used as substrates. Aluminium alloy was exposed to a three-step cleaning procedure using Metaclean T2001 (Chemie Vertrieb Hannover GmbH & Co KG), Turco Liquid Aluminetch Nr. 2 (Turco Chemie GmbH) and Turco Liquid Smutgo NC (Turco Chemie GmbH).

TMH sol (TEOS-MPS-HEMA) was synthesized keeping the molar ratio TEOS/MPS/HEMA of 60/10/30 following a two-step process based on a previous work [30]. In the first step, a solution of appropriate amounts of TEOS, MPS and 0.1N HNO_3 in ethanol at an equivalent concentration of 150 g L^{-1} SiO_2 was prepared. The concentration in the ethanol solution is expressed as the equivalent amount of SiO_2 in gram per Litre calculated on the basis of the amount of Si supplied both by TEOS and MPS. Hydrolysis and condensation reactions were produced at 50 °C for 1 h in a closed reactor. The amount of water supplied by the 0.1N HNO_3 solution was the stoichiometric one required for producing a complete hydrolysis and condensation through formation of Si–O–Si bonds (2 moles per mol of TEOS and 1.5 moles per mol of MPS). In the case of doped sols, the cerium salts were added at the end of this step of synthesis keeping a Ce/Si molar relation of 1/99 and 5/95. In the second step, appropriate amounts of HEMA and AIBN were added to the pre-condensed sol together with an extra amount of ethanol to reach the desired concentrations. The amount of AIBN was 0.01 moles per mol of C=C groups. The organic polymerization was produced at 65 °C in a closed reactor. Samples were extracted from the reactor at different reaction times and rapidly cooled to 5 °C to stop the organic and inorganic polymerization. These samples were used to monitor the evolution of the conversion and the viscosity of the sol as a function of time.

Hybrid sols were denoted as TMH sol and the SiO_2 concentration, expressed in gram per Litre, is included in the notation as TMH-50 and TMH-60. On the other hand, TMH-50 sols doped with Ce(III) ions were denoted expressing the salt concentration and kind as 1N-TMH-50 and 5N-TMH-50 for 1 and 5 molar % of cerium nitrate, respectively, and 1Cl-TMH-50 and 5Cl-TMH-50 for 1 and 5% of cerium chloride.

The evolution of the viscosity of different sols was measured at 25 °C by an Ostwald viscosimeter as a function of the polymerisation time during the second stage of the synthesis. Fourier Transformed Infrared Spectroscopy with Attenuated Total Reflectance (FTIR Vertex 70, Brücker, with ATR-Golden Gate Specac) was used to study the condensation of Si-O-Si during the first stage of the synthesis and the evolution of the C=C groups through the decreasing of the band at 1,639 cm^{-1} during the second stage in liquid samples, and the evaluation of residual Si-OH groups after the thermal treatment of the coatings. IR spectra were recorded between 400 and 4,000 cm^{-1}, with a resolution of 2 cm^{-1}. Spectra were deconvoluted trough Levenberg Marquardt algorithm using software OPUS Version 5.5 from Vertex 70 Standard Systems. Best fits were performed considering bands Gaussian/Lorentzian 60/40 approximately. Bandwidths were kept between 20 and 30 cm^{-1} while wavenumbers and intensities were allowed to vary. Residual RMS errors were around 0.001.

Coatings were obtained on both substrates by a conventional dip-coating process at withdrawal rates comprised between 5 and 60 cm min^{-1}. The coatings are prepared using a multilayer process, where each layer is drying for 15 min at room temperature before the deposition of a new layer. The coatings are made up of one, two or three layers. Finally, coatings were exposed to a thermal treatment of 120 °C during 60 min. Coating thickness was obtained by profilometry (Talystep, Taylor-Hobson UK) as a function of the withdrawal rate and polymerization degree. The C=C bonds after the thermal treatment of the coatings were measured by FTIR. Contact angles of water on the sol–gel coatings were measured using EasyDrop equipment (Kruss). Coating homogeneity and thickness was evaluated by scanning electron microscopy (HITACHI S-4700 field emission). Elemental chemical analysis of the coatings was performed by Energy Dispersive X-ray Spectroscopy (EDX, NORAN system six) connected to the FE–SEM. Electrochemical measurements on bare and coated substrates were performed in a 0.3 wt% NaCl solution with a conventional three-electrode cell. A

saturated calomel electrode (SCE) was used as reference and a platinum wire was used as counter-electrode. The working electrode area exposed to the electrolyte was 3.14 cm^2. The impedance measurements (EIS) were performed using a Gamry Fas2 Femtostat at different times of exposure to the electrolyte using sine wave signals of 5 mV rms amplitude. The measuring frequency ranged from 2×10^4 Hz down to 10^{-2} Hz. Each value was the mean value of five measurements in a logarithmic sweep of frequencies (10 points per logarithmic unit).

3 Results and discussion

Sols were transparent and colourless before the curing at 65 °C, and transparent and slightly yellowish after the treatment. Figure 1 shows the evolution of viscosity and polymerization of C=C groups of the TMH-50 and TMH-60 sols during the second step of synthesis at 65 °C. The TMH-50 sol presents slight changes until 160 min, after that the viscosity increases quickly becoming an unstable sol. On the other hand, the TMH-60 sol presents a faster increase of viscosity from the initial time. Although the organic polymerization takes place almost at the same rate in both sols, the gelling occurs later in the more diluted sol at higher conversion of C=C groups. This fact could be explained through the formation of microgels and the amount of solvent in the sol, which could lead to a 100% polymerized TMH sol without gelling [30].

Hybrid coatings after the thermal treatment appeared transparent, homogeneous and defect-free with a faint yellowish colour. Thickness (t) and withdrawal rate (v) in inorganic sol–gel coatings are related by $t \propto v^n$, where n is around 0.5 [31, 32]. The n values obtained in this work vary between 0.52 and 0.68 for each composition. These deviations are attributed to the rheological and flowing behaviour of the hybrid sols and the singular structure of their coatings [33]. The coating thickness increases with the curing time in the second step of synthesis because of the viscosity increase related with a greater extent of inorganic and organic polymerizations. TMH-50 sol was chosen for cerium doping and further characterization based on its higher stability.

Coatings thicker than 4 microns were obtained for multilayer coatings as the sum of thicknesses of single layers. In the case of inorganic sol–gel multilayer coatings, the thermal treatment before deposition of a new layer is

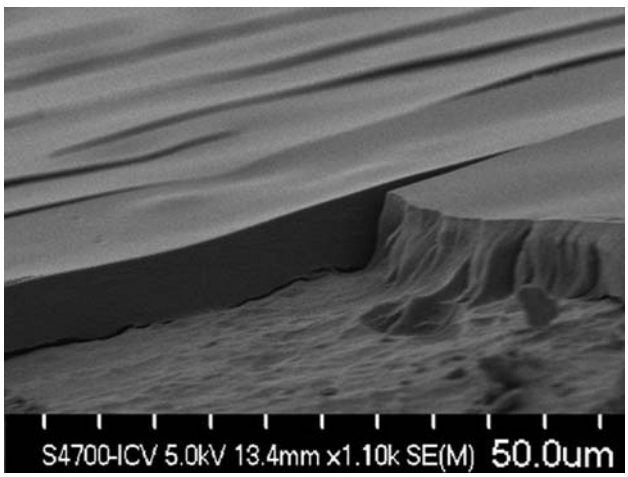

Fig. 2 SEM micrograph of a three-layer TMH-50 coating on AA2024 substrate

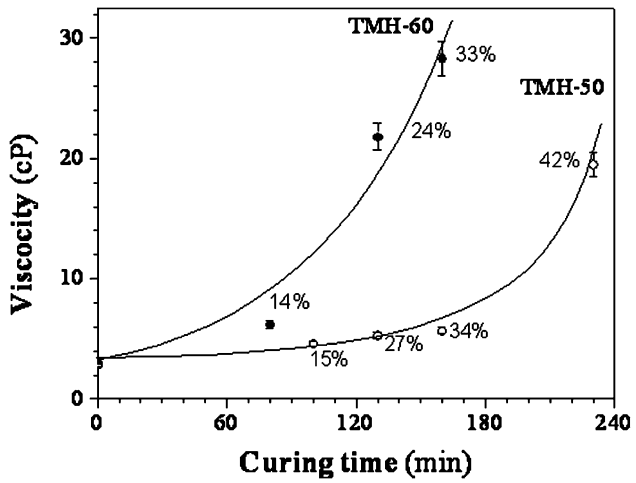

Fig. 1 Viscosity versus Curing time at 65 °C. The *organic polymerization percentages* are shown for each point

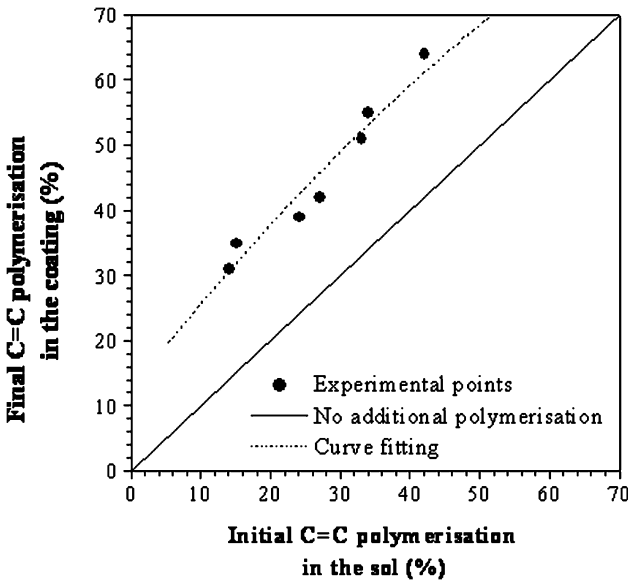

Fig. 3 Comparison of organic polymerization of TMH-50 sols and coatings after 1 h at 120 °C

essential to avoid debonding or dilution of the first layer. The possibility of synthesis of thick coatings using a multilayer process without intermediate high temperature thermal treatments is a very interesting way to obtain improved anticorrosion coatings.

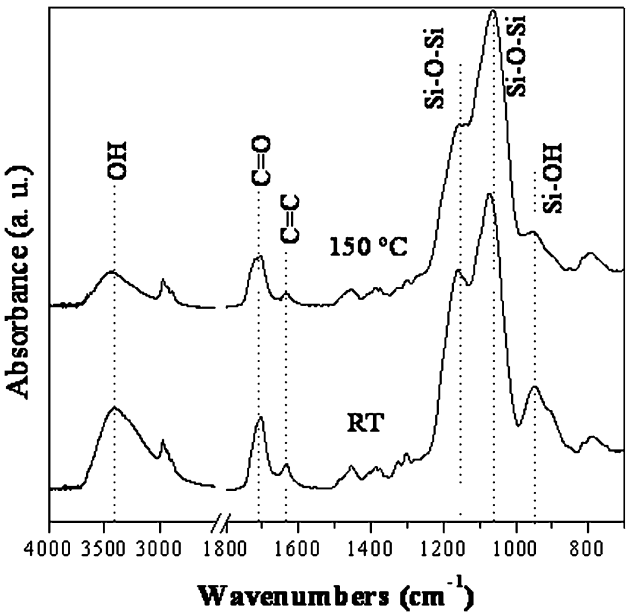

Fig. 4 ATR-FTIR spectra of the 1N-TMH-50 coating prepared with the 27% polymerized sol, and dried at room temperature and after the thermal treatment at 120 °C

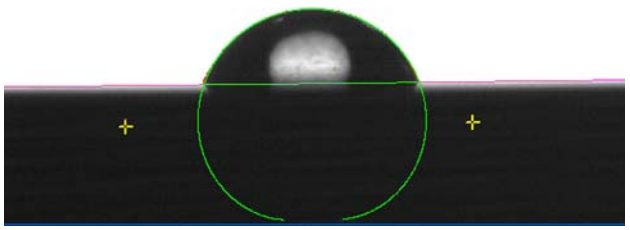

Fig. 5 Contact angle measurement of 1N-TMH-50 coatings after thermal treatment

Figure 2 shows an SEM micrograph of a transverse section of a three-layer coating prepared using the TMH-50 sol with a curing time of 160 min (34% polymerization degree) and a withdrawal rate of 53 cm min^{-1} on aluminium substrate. The figure presents the aluminium substrate with the coating on the top. Although the preparation of the sample for the SEM observation (cutting without insertion in resin) was highly aggressive and produced some cracks in the coating, the image demonstrates the good adherence existing between one layer and the others. In fact, it is impossible to detect any interface inside the coating. The thickness of the coating is around 5 μm, confirming the value obtained with glass substrates by profilometry.

The thermal treatment of the coatings to consolidate the structure produces an additional organic polymerization through cleavage of residual double bonds. Figure 3 shows the comparison of the polymerization achieved in the precursor sol with that in the coating after the 1 h thermal treatment at 120 °C. Other important result is that a high organic polymerization in the coating is obtained when it was advanced in liquid state, in the second step of sol synthesis [30].

Besides of the organic polymerization, the thermal treatment of coatings produces a growth of the inorganic network through condensation of Si-OR and Si-OH, which is strongly limited by steric impediment. Thus, although this additional condensation process requires the consumption of Si-OH groups, an important amount of those remain in the structure reinforcing the hydrophilic character conferred by hydroxyl groups of HEMA to the coating. Figure 4 shows the ATR-FTIR spectra, between 700 and 4000 cm^{-1}, of the 1N-TMH-50 coating prepared with the 27% polymerized sol, and dried at room temperature and after the thermal treatment at 120 °C. The assignation of the main bands appears in the figure, where a decreasing of the band associated with Si-OH bonds is observed. The contact angles measured on the thermal treated coatings show an average value of 69 ± 3°, which

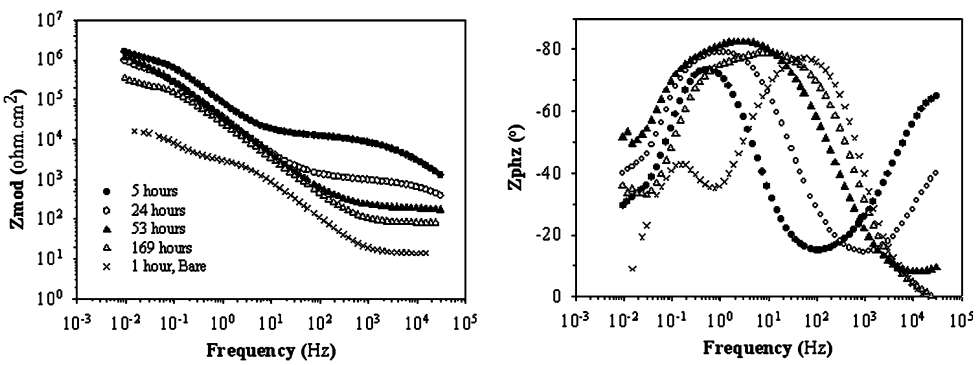

Fig. 6 EIS Bode plots for AA2024 alloys protected with a three-layer 1N-TMH-50 coating at different immersion times in 0.3 wt% NaCl compared with the bare substrate

could be low enough for the application of an water-base epoxy painting to provide barrier properties (Fig. 5).

The electrochemical impedance is a technique that has been widely used to predict the properties of various anti-corrosive coatings. Electrochemical analysis was performed for 1N, 1Cl and 5Cl coatings since 5N coatings presented initial defects compromising their integrity when observing to optical microscope. The impedance spectra of the coating 1N-TMH-50 with a thickness of 4.5 μm compared with the uncoated substrate are shown in Fig. 6. The curve of the phase angle of the bare AA2024 presents two maximum: one at 30 Hz correlated to the natural

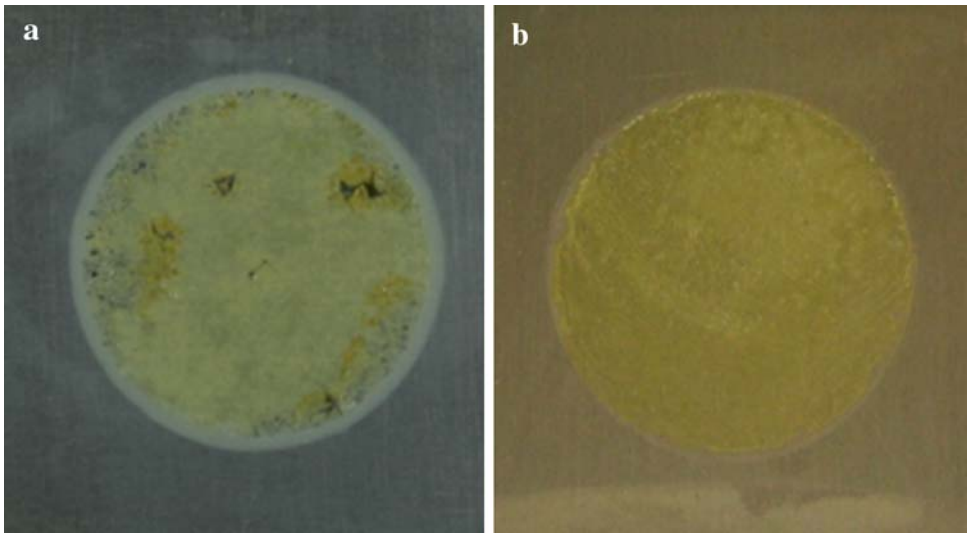

Fig. 7 Photographs of the AA2024 alloys protected with: **a** three-layer 1N-TMH-50 and **b** three-layer 5Cl-TMH-50 coatings, after approximately 170 h of immersion in 0.3 wt% NaCl solution

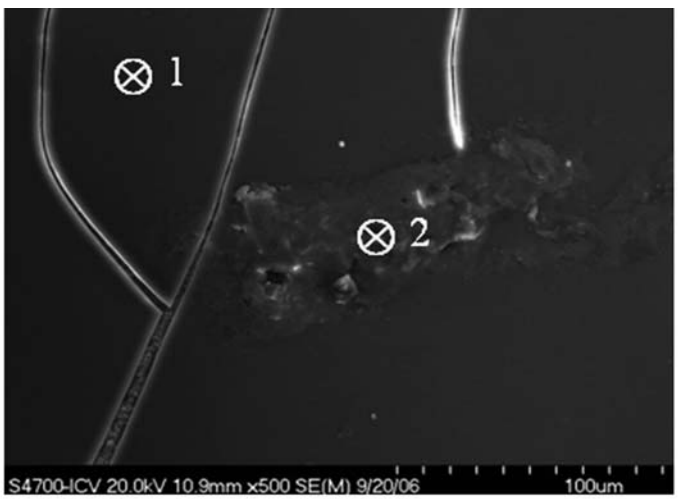

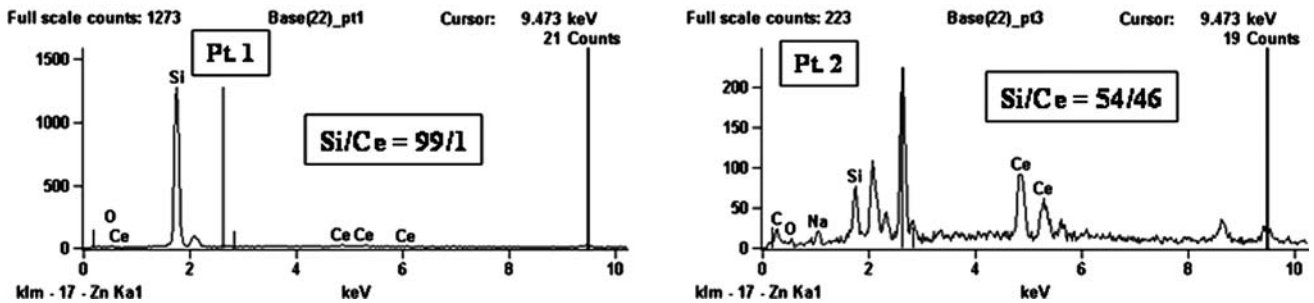

Fig 8 SEM EDS analysis after EIS test for 1N-TMH-50. It can be observed the higher Ce content in agglomerates when compared with the matrix (crosses on the SEM photomicrography mark the area where EDS test were performed)

aluminium oxide and the other at 0.15 Hz assigned to the charge transfer process [25, 28, 29]. It is possible to notice that the sol–gel coating introduces a new time constant at higher frequencies, above 10^4 Hz. The value of the impedance modulus at low frequencies (0.01 Hz) is a simple parameter that can be used to compare the protection provided by different systems against corrosion; a higher impedance value corresponds to a better protection. This coating presents an impedance modulus value at low frequencies close to 10^6 Ω cm^2, two orders of magnitude higher than that of the uncoated substrate. The phase angle curve after 5 h of immersion shows two time constants: above 10^4 Hz and around 0.4 Hz associated with the sol–gel coating and the aluminium oxide layer, respectively. At lower frequencies (around 0.03 Hz) the phase angle increases slightly, suggesting the occurrence of diffusion processes within pores in the coating. This behaviour can be related with the first signal of corrosion activity. The study of impedance evolution with immersion time also allows estimating the mechanisms associated with the incorporation of cerium. The TMH coating has a high hydrophilic character and porosity volume associated with the terminal OH groups from HEMA and un-condensate

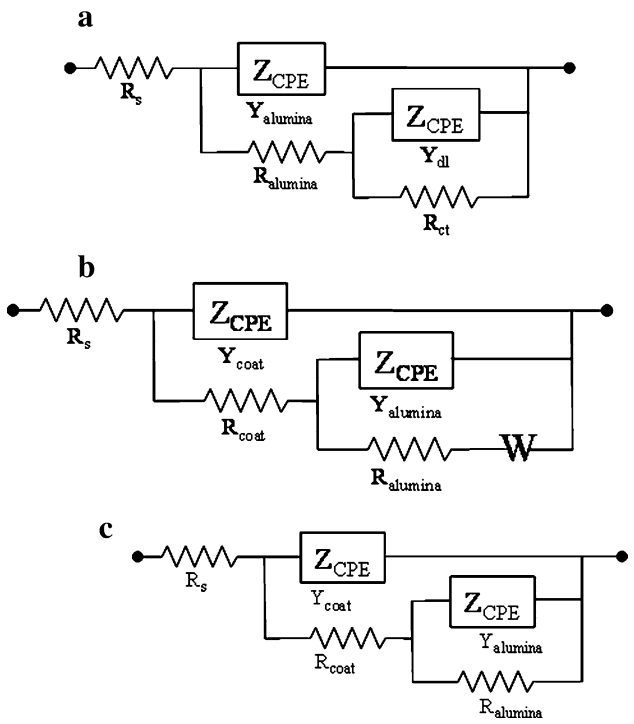

Fig. 9 Equivalent circuits used to fit the EIS spectra: **a** Bare AA2024 after 2 h of immersion; AA2024 with a three-layer 1N-TMH-50 coating after 169 h of immersion, AA2024 with a three-layer 5Cl-TMH-50 coating after 168 h of immersion **b** AA2024 with a three-layer 1N-TMH-50 coating after 5, 24 and 53 h of immersion; AA2024 with a three-layer 5Cl-TMH-50 coating after 30 h of immersion **c** AA2024 with a three-layer 5Cl-TMH-50 coating after 1 and 5 h of immersion with a three-layer

Table 1 Fitting parameters for AA2024 alloy protected with a three-layer 1N-TMH-50 coating using the equivalent circuits shown in Fig. 9

Sample, time	R_s (ohm. cm^2)	Y_{coat} (S s^a cm^{-2})	a_{coat}	R_{coat} (ohm.cm^2)	$Y_{alumina}$ (S s^a cm^{-2})	$a_{alumina}$	$R_{alumina}$ (ohm.cm^2)
Bare, 2 h	43.77 ± 0.19				$7.11 \times 10^{-6} \pm 7.85 \times 10^{-8}$	$0.94 \pm 1.71 \times 10^{-3}$	$1.02 \times 10^4 \pm 1.28 \times 10^2$
Coated, 5 h	81.2	$6.77 \times 10^{-8} \pm 8.17 \times 10^{-9}$	$0.77 \pm 1.07 \times 10^{-2}$	$1.27 \times 10^4 \pm 3.27 \times 10^2$	$2.14 \times 10^{-6} \pm 7.09 \times 10^{-8}$	$0.91 \pm 1.02 \times 10^{-2}$	$1.36 \times 10^6 \pm 1.06 \times 10^5$
Coated, 24 h	81.2	$4.43 \times 10^{-7} \pm 7.18 \times 10^{-8}$	$0.71 \pm 1.02 \times 10^{-2}$	$1.07 \times 10^3 \pm 2.41 \times 10^1$	$4.85 \times 10^{-6} \pm 1.58 \times 10^{-7}$	$0.91 \pm 6.01 \times 10^{-3}$	$9.22 \times 10^5 \pm 6.1 \times 10^4$
Coated, 53 h	81.2	$7.94 \times 10^{-7} \pm 1.76 \times 10^{-7}$	$0.69 \pm 3.02 \times 10^{-2}$	$1.56 \times 10^2 \pm 5.07$	$4.73 \times 10^{-6} \pm 3.21 \times 10^{-7}$	$0.92 \pm 1.01 \times 10^{-2}$	$1.53 \times 10^6 \pm 2.18 \times 10^5$
Coated, 169 h	82.18 ± 0.44				$7.58 \times 10^{-6} \pm 3.57 \times 10^{-8}$	$0.89 \pm 0.95 \times 10^{-3}$	$2.79 \times 10^5 \pm 1.81 \times 10^3$

Sample, time	Y_{dl} (S s^a cm^{-2})	a_{dl}	R_{ct} (ohm.cm^2)	W–R	W–T	W–P
Bare, 2 h	$6.16 \times 10^{-5} \pm 6.80 \times 10^{-7}$	$0.87 \pm 1.40 \times 10^{-2}$	$4.81 \times 10^4 \pm 2.52 \times 10^3$			
Coated, 5 h				$1.37 \times 10^6 \pm 3.95 \times 10^5$	57.4 ± 9.54	$0.77 \pm 1.08 \times 10^{-2}$
Coated, 24 h				$1.0810^6 \pm 2.42 \times 10^5$	60.95 ± 11.3	$0.72 \pm 5.74 \times 10^{-3}$
Coated, 53 h				$3.08 \times 10^6 \pm 1.44 \times 10^5$	83.54 ± 7.71	$0.84 \pm 6.77 \times 10^{-2}$
Coated, 169 h	$8.47 \times 10^{-5} \pm 1.48 \times 10^{-6}$	0.99 ± 0.01	$4.9 \times 10^5 \pm 3.08 \times 10^4$			

silanol groups. This structure allows an easy penetration of the aqueous solution through the pores. Therefore, the electrolyte reaches the substrate after a short time producing a fast degradation of the system. The incorporation of inhibitors can reduce this effect introducing an additional protection system.

The increasing of the immersion time up to 53 h clearly shows a new time constant at low frequencies associated to corrosion activity due to the porous structure of TMH coating. The deterioration of the protection system with increasing immersion time is reflected in the drop of the values of impedance modulus at high frequencies. Despite this, the value of the impedance at 0.01 Hz after 53 h is slightly higher compared to the 24 h curve. The increase of low frequency impedance in the case of inhibitor-containing coating has been related for different authors to the partial recovery of the oxide film and to the partial suppression of the corrosion activity in the defect [25, 29]. The role of cerium ions on the protection against corrosion has been associated with the precipitation of cerium hydroxides/oxide on cathode sites [20, 25, 28, 29, 34–36]. Some works [17, 18, 34, 35] described the partial oxidation of ions Ce^{3+} to Ce^{4+}, and the subsequent precipitation of CeO_2 with a high concentration of Ce through intermediate species of $Ce(OH)_2^+$ or $Ce(OH)_3$. In our case, at the end of the test, the sample presents yellow precipitates as a signal of the protective role of the cerium ions (Fig. 7a). SEM-EDS (Fig. 8) analysis of the surface after the EIS-time test shows a higher Ce concentration compared with the nominal one in some particle agglomerates. However, the cerium analysis does not show a homogeneous distribution. This behaviour can be attributed to some kind of self-healing effect provided by cerium ions in specific areas. The degradation of the coating after 169 h of immersion is clearer, reflected in the drop of the impedance modulus at high and low frequencies and the loss of the maximum in the angle plot at high frequencies. The TMH structure facilitates the mobility of cerium through the coating, but also allows the penetration of the aqueous electrolyte. Nevertheless, the additional protection of cerium could explain the remaining high total impedance values. On the other hand, these coatings would be only a pre-treatment with the main function of providing an inhibition action where the external coatings (paintings) that work as a barrier against the electrolyte would suffer damage. As the 1Cl-TMH-50 coating performs with a similar behaviour, the corresponding impedance spectra are not shown in order to facilitate the reading of the manuscript.

The interpretation of impedance spectra was performed using numerical fitting. In the simulation, the constant phase element (Z_{CPE}) was used instead of an "ideal" capacitor to explain the deviations from ideal behaviour. The Z_{CPE} can be defined by $Z_{CPE} = (1/Y)/(jw)^a$ which parameters are the frequency (w), pseudo-capacitance (Y), and the parameter a associated to the system homogeneity. The equivalent circuits used to model the impedance curves of 1N-TMH-50 coating are displayed in Fig. 9, where R_s is the resistance of the electrolyte, R_{coat} the resistance of the sol–gel coating, Y_{coat} is the pseudo-capacitance of the sol–gel coating, $R_{alumina}$ and $Y_{alumina}$ the resistance and pseudo-capacitance associated with the thin natural aluminium oxide layer, R_{ct} the resistance describing the corrosion of the metal substrate and Y_{dl} the double-layer pseudo-capacitance formed in the metal-electrolyte interface. Warburg impedance is used to model increasing ionic conductivity due to corrosion processes occurring inside the pores and the increasing diffusivity into them. If the material is thin, low frequencies will penetrate the entire thickness, creating a finite length Warburg element (Eq. 1) [36].

$$Z_w = \frac{R_{DO}}{(jT\omega)^p} \tan h(jT\omega)^p \quad (1)$$

where R_{DO} (W–R) is associated with solid phase diffusion and T (W–T) is related to diffusion coefficient and pore length. As the phase angle decreases at low frequencies without reaching a zero value, it suggested the presence of pores in the outer part of the coating and diffusion effects inside.

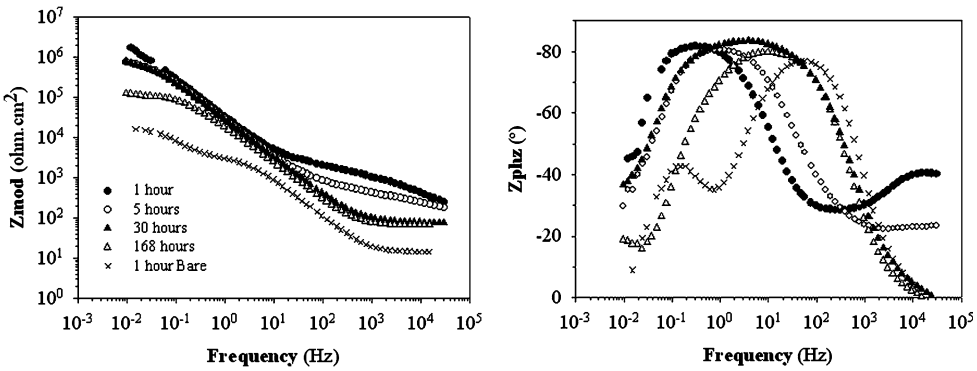

Fig. 10 EIS Bode plots for AA2024 alloys protected with a three-layer 5Cl-TMH-50 coating at different immersion times in 0.3 wt% NaCl compared with the bare substrate

Table 1 shows the fitting of the data for the models presented in Fig. 9. R_{coat} reduction and Y_{coat} increasing can be associated with the water uptake through pores and defects in the coating producing the deterioration of the protection system. This is also evidenced by the shift of the high frequency maxima to higher frequencies. W–R and W–T for the system slightly increase after 53 h of immersion. It can be related to the "plugging" of oxide/hydroxide products through the pores making diffusion more difficult and this, in turn, although small, could be associated to some kind of self sealing effect. Conversely, the increase in $R_{alumina}$ can be associated to a decrease of exposed area due to the deposits. Even the corrosion process after 169 h of immersion is evident, the higher value of R_{ct} compared with the bare substrate indicates still the existence of some protection after the immersion.

Figure 10 shows the Bode plots for 5Cl-TMH-50 coating with a thickness of 4.5 μm compared with the bare substrate. The values of impedance at short immersion time indicate a less protective behaviour compared to that obtained with the 1N-TMH-50 coating. It is possible that the increasing of cerium concentration in the coating generates a greater number of defects [37] and, consequently, an acceleration of the corrosion process in the absence of an additional coating as a barrier (paintings) considering that both present the same thickness. Nevertheless, the total impedance remains constant up to 30 h. At this time, two close time constants appear and the angle drop at low frequencies tending to a constant value can be related to a diffusion effect. The time constant a high frequency can be related to the coating properties and the one at lower frequencies to corrosion processes that occurs through the defects. After longer immersion time, 168 h, the impedance at low frequency decreases and the corrosion activity becomes well defined. The diffusion limitations arise most likely due to formation of a layer of corrosion products on the corroded zone. The Fig. 7b presents the coating after the impedance test, showing yellow precipitates that are identified as cerium oxide by EDS and associated to the cerium ion protection role. The equivalent circuits used to model the impedance curves of 5Cl-TMH-50 coating are displayed in Fig. 9, and the fitting of the data are shown in Table 2.

4 Conclusions

Organic-inorganic hybrid sol–gel coatings with a high organic content and controlled polymerization have been prepared. The coatings have been doped with cerium ions trying to provide active protection through a process of self-healing by the precipitation of cerium oxides/hydroxides. The control of the inorganic and organic

Table 2 Fitting parameters for AA2024 alloy protected with a three-layer 5Cl-TMH-50 coating using the equivalent circuits shown in Fig. 9

Sample, time	R_s (ohm.cm^2)	Y_{coat} (S s^a cm^{-2})	a_{coat}	R_{coat} (ohm.cm^2)	$Y_{alumina}$ (S s^a cm^{-2})	$a_{alumina}$	$R_{alumina}$ (ohm.cm^2)
Bare, 2 h	43.77 ± 0.19				$7.11 \times 10^{-6} \pm 7.85 \times 10^{-8}$	0.94 ± 1.71 × 10^{-3}	$1.02 \times 10^4 \pm 1.28 \times 10^2$
Coated, 1 h	87	$1.27 \times 10^{-6} \pm 2.04 \times 10^{-7}$	0.69 ± 1.40 × 10^{-2}	$2.23 \times 10^3 \pm 1.00 \times 10^2$	$3.97 \times 10^{-6} \pm 2.27 \times 10^{-7}$	0.95 ± 1.33 × 10^{-2}	$3.37 \times 10^6 \pm 4.61 \times 10^5$
Coated, 5 h	87	$1.09 \times 10^{-6} \pm 1.96 \times 10^{-7}$	0.74 ± 1.50 × 10^{-2}	$4.33 \times 10^3 \pm 1.53 \times 10^1$	$5.77 \times 10^{-6} \pm 1.63 \times 10^{-7}$	0.89 ± 3.21 × 10^{-3}	$1.08 \times 10^6 \pm 6.41 \times 10^4$
Coated, 30 h	76.55 ± 0.18	$5.08 \times 10^{-6} \pm 7.65 \times 10^{-8}$	0.93 ± 1.04 × 10^{-3}	$2.10 \times 10^2 \pm 9.82 \times 10^1$	$2.01 \times 10^{-6} \pm 7.32 \times 10^{-7}$	0.91 ± 2.65 × 10^{-2}	$7.81 \times 10^5 \pm 2.08 \times 10^4$
Coated, 168 h	66.39 ± 0.40				$9.90 \times 10^{-6} \pm 7.02 \times 10^{-8}$	0.91 ± 1.46 × 10^{-3}	$1.16 \times 10^5 \pm 9.82 \times 10^2$
Sample, time	Y_{dl} (S s^a cm^{-2})	a_{dl}	R_{ct} (ohm.cm^2)	W–R	W–T	W–P	
Bare, 2 h	$6.16 \times 10^{-5} \pm 6.80 \times 10^{-7}$	0.87 ± 1.40 × 10^{-2}	$4.81 \times 10^4 \pm 2.52 \times 10^3$				
Coated, 1 h							
Coated, 5 h							
Coated, 30 h				$3.04 \times 10^6 \pm 1.39 \times 10^5$	214.9 ± 5.27	0.92 ± 6.55 × 10^{-3}	
Coated, 168 h	$3.97 \times 10^{-4} \pm 1.82 \times 10^{-5}$	0.97 ± 3.78 × 10^{-3}	$7.20 \times 10^4 \pm 3.27 \times 10^3$				

polymerization process allows the preparation of 5 microns thickness multilayer coatings with an open structure to facilitate the mobility of cerium ions through the structure.

Electrochemical measurements evidence good barrier properties at initial immersion time with impedance modulus values at low frequencies of 10^6 Ω cm^2, two orders of magnitude higher than that of the uncoated substrate. Signals of corrosion inhibition provided by cerium ions at long immersion times could be associated with the increase of impedance at low frequencies and the presence of yellow precipitates with a high concentration of cerium, although additional tests are required to confirm this property. A promising protection system could be integrated by these sol–gel cerium doped coatings and paintings (topcoat and primer) in order to combine its barrier properties with the corrosion inhibition of the former.

Acknowledgments Authors acknowledge the funding provided by the European Community (MULTIPROTECT project: "Advanced environmentally friendly multifunctional corrosion protection by nanotechnology", Contract No NMP3-CT-2005-011783), the Spanish Ministry of Education and Science (projectMAT2006-4375) and the National Research Council of Argentina (CONICET). The authors thank Laura Pelaéz and Eva Peiteado their assistance with the experimental technique.

References

1. Voevodin N, Jeffcoate C, Simon L, Khobaib M, Donley M (2001) Surf Coat Tech 140:29. doi:10.1016/S0257-8972(01)01000-3
2. Hughes AE, Taylor RJ (1997) Surf Interface Anal 25:223. doi:10.1002/(SICI)1096-9918(199704)25:4<223::AID-SIA225>3.0.CO;2-D
3. Baral A, Engelken R, Stephens W, Farris J, Hannigan R (2006) Arch Environ Contam Toxicol 50:496. doi:10.1007/s00244-005-0068-x
4. Bethencourt M, Botana FJ, Calvino JJ, Marcos M, Rodriguez-Chacon MA (1998) Corros Sci 40:1803. doi:10.1016/S0010-938X(98)00077-8
5. Arenas MA, Bethencourt M, Botana FJ, Damborenea JJ, Marcos M (2001) Corros Sci 43:157. doi:10.1016/S0010-938X(00)00051-2
6. Arenas MA, Conde A, Damborenea JJ (2002) Corros Sci 44:511. doi:10.1016/S0010-938X(01)00053-1
7. Hughes AE, Taylor RJ, Hinton BRW, Wilson L (1995) Surf Interface Anal 23:540. doi:10.1002/sia.740230714
8. Hinton BRW (1992) J Alloys Comp 180:15. doi:10.1016/0925-8388(92)90359-H
9. Kendig MW, Buchheit RG (2003) Corrosion 59:379
10. Durán A, Castro Y, Aparicio M, Conde A, Damborenea JJ (2007) Int Mater Rev 52(3):175. doi:10.1179/174328007X160263
11. Conde A, Durán A, Damborenea JJ (2002) Bol Soc Esp Ceram Vidr 41(3):319
12. Conde A, Durán A, Damborenea JJ (2003) Prog Org Coat 46(4):286. doi:10.1016/S0300-9440(03)00014-6
13. Voevodin NN, Grebasch NT, Soto WS, Kasten L, Grant JT, Arnold TE, Conley MS (2001) Prog Org Coat 41:287. doi:10.1016/S0300-9440(01)00156-4
14. Khobaib M, Reynolds LB, Donely MS (2001) Surf Coat Tech 140:16. doi:10.1016/S0257-8972(01)00998-7
15. Vreugdenhil AJ, Gelling VJ, Woods ME, Schmelz JR, Enderson BP (2008) Thin Solid Films 517:538. doi:10.1016/j.tsf.2008.06.073
16. Woods ME, Vreugdenhil AJ (2006) J Mater Sci 41:7545. doi:10.1007/s10853-006-0839-4
17. Pepe A, Aparicio M, Durán A, Ceré S (2006) J Sol-Gel Sci Technol 39(2):131. doi:10.1007/s10971-006-9173-1
18. Pepe A, Aparicio M, Ceré S, Durán A (2004) J Non-Cryst Solids 348:162. doi:10.1016/j.jnoncrysol.2004.08.141
19. Trabelsi W, Triki E, Dhouibi L, Ferreira MGS, Zheludkevich ML, Montemor MF (2006) Surf Coat Tech 200:4240. doi:10.1016/j.surfcoat.2005.01.044
20. Trabelsi W, Cecilio P, Ferreira MGS, Montemor MF (2005) Prog Org Coat 54:276. doi:10.1016/j.porgcoat.2005.07.006
21. Voevodin NN, Grebasch NT, Soto WS, Arnold FE, Donley MS (2001) Surf Coat Tech 140:24. doi:10.1016/S0257-8972(01)00999-9
22. Kasten LS, Grant JT, Grebasch N, Voevodin N, Arnold FE, Donley MS (2001) Surf Coat Tech 140:11. doi:10.1016/S0257-8972(01)01004-0
23. Zheludkevich ML, Serra R, Montemor MF, Yasakau KA, Miranda Salvado IM, Ferreira MGS (2005) Electrochim Acta 51:208. doi:10.1016/j.electacta.2005.04.021
24. Osborne JH, Blohowiak KY, Taylor SR, Hunter C, Bierwagon G, Carlson B, Bernard D, Donley MS (2001) Prog Org Coat 41:217. doi:10.1016/S0300-9440(01)00132-1
25. Zheludkevich ML, Serra R, Montemor MF, Miranda Salvado IM, Ferreira MGS (2006) Surf Coat Tech 200:3084. doi:10.1016/j.surfcoat.2004.09.007
26. Liu Y, Sun D, You H, Chung JS (2005) Appl Surf Sci 246:82. doi:10.1016/j.apsusc.2004.10.040
27. López DA, Rosero-Navarro NC, Ballarre J, Durán A, Aparicio M, Ceré S (2008) Surf Coat Technol 202:2194. doi:10.1016/j.surfcoat.2007.09.007
28. Zheludkevich ML, Yasakau KA, Bastos AC, Karavai OV, Ferreira MGS (2007) Electrochem Commun 9:2622. doi:10.1016/j.elecom.2007.08.012
29. Rosero-Navarro NC, Pellice SA, Duran A, Aparicio M (2008) Corros Sci 50:1283. doi:10.1016/j.corsci.2008.01.031
30. Pellice SA, Williams RJJ, Sobrados I, Sanz J, Castro Y, Aparicio M, Durán A (2006) J Mater Chem 16:3318. doi:10.1039/b605693h
31. Strawbridge I, James PF (1986) J Non-Cryst Solids 86:381. doi:10.1016/0022-3093(86)90026-8
32. Guglielmi M, Zenezini S (1990) J Non-Cryst Solids 121:303. doi:10.1016/0022-3093(90)90148-F
33. Pellice SA, Galliano P, Castro Y, Durán A (2003) J Sol-Gel Sci Technol 28:81. doi:10.1023/A:1025641204648
34. Aldykiewicz AJ, Davenport AJ, Isaacs HS (1996) J Electrochem Soc 143:147. doi:10.1149/1.1836400
35. Arenas MA, Damborenea JJ (2003) Electrochim Acta 48:3693. doi:10.1016/S0013-4686(03)00507-3
36. Z plot for windows, electrochemical impedance software operating manual. Part I, Scribner Associates, Inc., Southern Pines, NC (1998)
37. Zheludkevich ML, Shchukin DG, Yasakau KA, Möhwald H, Ferreira MGS (2007) Chem Mater 19:402. doi:10.1021/cm062066k